

Superiority of L-tartaric Acid Modified Chiral Mesoporous Silica Nanoparticle as a Drug Carrier: Structure, Wettability, Degradation, Bio-Adhesion and Biocompatibility

This article was published in the following Dove Press journal:
International Journal of Nanomedicine

Beibei Hu^{1,2}
Jianxin Wang³
Jing Li³
Sanming Li³
Heran Li¹

¹School of Pharmacy, China Medical University, Shenyang 110122, People's Republic of China; ²College of Chemistry and Pharmaceutical Engineering, Hebei University of Science and Technology, Shijiazhuang 050018, People's Republic of China; ³School of Pharmacy, Shenyang Pharmaceutical University, Shenyang 110016, People's Republic of China

Purpose: The purpose of this research was to study the basic physicochemical and biological properties regarding the application of L-tartaric acid modified chiral mesoporous silica nanoparticle (CMSN) as a drug carrier, and to explore the structure–property relationship of silica-based materials.

Methods: CMSN with functions of carboxyl modification and chirality was successfully synthesized through co-condensation method, and the basic characteristics of CMSN, including morphology, structure, wettability, degradation, bio-adhesion and retention ability in gastrointestinal tract (GI tract) were estimated by comparing with non-functionalized mesoporous silica nanoparticles (MSN). Meanwhile, the biocompatibility and toxicity of L-tartaric modification were systematically evaluated both in vitro and in vivo through MTT cell viability assay, cell cycle and apoptosis assay, hemolysis assay, histopathology examination, hematology analysis, and clinical chemistry examination.

Results: CMSN and MSN were spherical nanoparticles with uniform mesoporous structure. CMSN with smaller pore size and carboxyl functional groups exhibited better wettability. Besides, CMSN and MSN could dissolve thoroughly in simulated physiological fluids during a degradation period of 1–12 weeks. Interestingly, the in vitro and in vivo behaviors of carriers, including degradation, bio-adhesion and retention ability in the GI tract were closely related to wettability. As expected, CMSN had faster degradation rate, higher mucosa-adhesion ability, and longer retention time. Particularly, CMSN improved the bio-adhesion property in both gastric mucosa and small intestinal mucosa, and prolonged the GI tract retention time to at least 12 h, which meant higher probability for absorption. The biocompatibility and toxicity examination indicated that CMSN was a kind of biocompatible bio-material with good blood compatibility and negligible toxicity, which is required for further applications in biological fields.

Conclusion: CMSN with functions of carboxyl modification and chirality had superiority in terms of both physicochemical and biological properties. The in vitro and in vivo behaviors of carriers, including degradation, bio-adhesion, and retention were closely related to wettability.

Keywords: chiral mesoporous silica, carboxyl modification, wettability, bio-adhesion, biocompatibility

Correspondence: Heran Li
School of Pharmacy, China Medical University, 77 Puhe Road, Shenyang North New Area, Shenyang 110122, People's Republic of China
Tel +86 13897945866
Email liheranmm@163.com

Introduction

Since the discovery of M41_S in the early 1990s, mesoporous silica nanoparticles (MSNs) with a pore size ranging from 2 nm to 50 nm have attracted much attention and have served as efficient drug delivery systems for various therapeutic agents.^{1–5}

Different from the traditional drug carriers such as micelles, organic gels and liposomes, MSNs with inorganic rigid structural framework exhibit chemical inertness, mechanical strength and thermal stability, and could effectively protect their cargo from premature degradation and chemical/biological reactions under rigorous physiological conditions, and can deliver a large amount of cargo in a controlled manner during their transportation *in vivo*.^{6–8} As mesoporous materials, their internal nanopores with large surface area and pore volume provide great potential for drug adsorption and loading, while the silanol enriched external surfaces are easily modified with molecular, supramolecular or polymer moieties, and could improve the versatility of carriers.^{1,5,6} Moreover, the tunable nanometer-sized pore size of MSNs effectively reduce the particle size of cargo and provide better control of drug loading and release kinetics while performing delivery tasks.^{1,3,9}

A substantial number of studies have reported the applications of MSNs as drug carriers, and the use of MSNs as drug carriers have been proven to be successful *in vitro*.^{6–8,10–12} To the best of our knowledge, the efficacy of MSN carriers is decided by the structural features which determine the physicochemical properties of MSNs, including shape, size, pore characteristics, and surface chemistry.¹³ Along with great progress in the structure control and multi-functionalization design of MSNs, various drug delivery formulations such as immediate drug delivery systems, sustained drug delivery systems, controlled drug delivery systems, targeted drug delivery systems, and stimuli-responsive drug delivery systems have been developed to improve the dissolution and bioavailability of poorly water-soluble drugs and enhance their therapeutic potential.^{9–12,14,15}

It should be noted that, a slight change in structural features of MSNs may not only significantly influence their host-guest interactions with drug molecules, but also impact the biological binding ability with tissues and cells.^{4,16} For example, Lu et al demonstrated that decreasing the size of NPs (from 50–280 nm) is an effective way to facilitate the cell uptake of MSNs.¹⁷ Li et al studied the effect of aspect ratios (AR) on *in vivo* behaviors of MSNs, and found that with the increase of AR, MSNs showed decreased systematic absorption, excretion, and *in vivo* biodegradation.¹⁸ Furthermore, modified MSNs with adjustable surface chemistry are widely used in drug delivery, because the functional groups can improve the biocompatibility, enhance the adsorption capacity to guest molecules, and increase the interactions

with tissues and cells.^{16,19} Thorough understanding of the relationship between fundamental characteristics and *in vivo* behaviors of MSNs is urgently needed for their future clinical application and of great importance to improve the performance of nano-materials.

As one of the most critical structural characteristics, chirality is found universally in nature, and acts as an inherent feature of most molecular and macromolecular components.²⁰ Also, the synthesis and potential applications of chiral mesoporous silicas (CMSs) have attracted much attention due to their unique advantages in the related fields of physics, materialogy, biology, and medicine.^{20,21} However, little attention has been paid to the drug delivery system based on CMSs. Recently, a new kind of CMSN was synthesized by our group through co-condensation method by using a synthesized chiral silane coupling agent called APTTES, consisting of 3-aminopropyltriethoxysilane (APTES) and L-tartaric.^{22,23} As a kind of silica-based material, it had potential value to be employed as drug carrier and would further expand the application areas of MSNs due to its chiral nature. Our previous studies have indicated that drugs could be loaded into CMSN (called Carboxyl-CMS in that report) with high efficiency in amorphous form, and the drug release rate was significantly increased.²² Specifically, CMSN exhibited pH-response controlled release performance owing to the negatively charged carboxyl modification groups.²³ These results demonstrated that CMSN had undertaken the mission of being a drug carrier and showed superiority in controlling the drug loading and release kinetics.

In the present study, our work mainly focused on how to rationally take advantage of the structural characteristics and biological effects of CMSN. The basic characteristics of CMSN including morphology, structure, and wettability were estimated by using transmission electron microscope (TEM), scanning electron microscope (SEM), Fourier transform infrared spectrometer (FTIR), circular dichroism apparatus (CD), small-angle X-ray diffractometer (SAXS), nitrogen adsorption and desorption tests and contact angle measurement, and were compared with MSN (without surface modification). *In vitro* biodegradation studies of CMSN and MSN were carried out in simulated gastric fluid (SGF, pH 1), simulated intestinal fluid (SIF, pH 6.8), and simulated body fluid (SBF, pH 7.4), over a time period of 12 weeks. Besides, bio-adhesive property and the GI tract retention ability of these engineered MSNs were systematically studied to explore the mechanism of promoting absorption. Finally, since unmodified MSN had

been proven to be biocompatible, the biocompatibility of CMSN was evaluated both *in vitro* and *in vivo* through MTT cell viability assay, cell cycle and apoptosis assay, hemolysis assay, histopathology analysis, hematology examination, and clinical chemistry examinations. It is believed that the study would contribute to understanding the structure–property relationship of bio-materials and bring new insights to the rational design of drug delivery systems.

Materials and Methods

Materials

Cetyltrimethyl ammonium bromide (CTAB), APTES, and L-tartaric acid were purchased from Aladdin (Shanghai, China). Tetraethoxysilane (TEOS), polyethyleneimine (PEI), and citric acid (CA) were obtained from Chengdu Xiya Chemical Technology Co., Ltd. (Chengdu, China). 3-(4,5-dimethylthiazol-2-yl)-2,5-diphenyltetrazolium bromide (MTT) and the cell cycle and apoptosis analysis kit were provided by the Beyotime Institute of Biotechnology (Shanghai, China). All other chemicals were of reagent grade and used without any further purification.

Synthesis of MSN and CMSN

MSN and CMSN were synthesized according to the previous papers.^{22,23} CMSN was prepared through a one-pot synthetic procedure by using CTAB as template, APTTES as co-structure directing agent, and TEOS as silica source. APTTES was prepared by combining L-tartaric with APTES. Briefly, 0.5 mL APTES was dispersed into 20 mL L-tartaric acid solution (1 mol/L) with gentle stirring for 4 h, and the product APTTES was separated by filtration. Then 0.8 g CTAB was dissolved into the mixture of 100 mL water and 30 mL ethanol followed by the addition of 0.8 mL ammonia and 0.5 g APTTES. 2.5 mL TEOS was added dropwise to the system under stirring conditions for 4 h to get the homogeneous solution. Afterwards, the reaction mixture remained static for 24 h, was separated by centrifugation, washed, dried and finally refluxed in a methanol solution of HCl (0.1 mol/L) to remove the template.

MSNs were synthesized through the same procedure, except no APTTES was introduced.

Structural Characterization

FTIR (Spectrum 1000, Perkin Elmer, USA) spectra of samples (APTES, MSN and CMSN) were recorded from 400–4000 cm^{-1} to study the structural information.

Meanwhile, the chirality features of MSN and CMSN were determined using MOS-500 CD apparatus (Bio-Logic, France). The morphology and detailed mesoscopic structure of MSN and CMSN were obtained by a TEM instrument (Tecnai G2-F30, FEI, the Netherlands) and an SEM instrument (JSM-6510A, JEOL, Japan). The nitrogen adsorption-desorption isotherms and the texture parameters including the specific surface area (S_{BET}), pore size distributions (W_{BJH}), and total pore volume (V_t) of samples were analyzed using a surface area and pore size analyzer (V-Sorb 2800P, Gold APP, China). Brunauer–Emmett–Teller (BET) method was utilized to calculate the surface area, and Barrett–Joyner–Halenda (BJH) method was employed to evaluate the W_{BJH} of samples. The SAXD patterns were acquired from an X-ray diffractometer (EMPYREAN, PANalytical, the Netherlands) equipped with a Ni-filtered CuK α line. Data were collected from 0.7° to 10° (diffraction angle 2 θ).

Wettability Measurement

To investigate the interfacial properties of MSN and CMSN, wettability measurement was carried out. The contact angles of carriers were determined using a model JCY series drop angle apparatus and sessile drop method (Shanghai, China). In detail, 200 mg MSN and CMSN were respectively compressed into tablets. For each case, a droplet of water was carefully exposed to the tablet, and the wettability procedure was imaged by a high-resolution CCD digital camera. Photos were then transferred to a computer, and the contact angles of samples were measured using tangent method. Since MSN and CMSN were a kind of porous material which exhibited complex interfacial behaviors, both the initial contact angles and the equilibrium contact angles were investigated. The measurement was performed in triplicate.

Besides, wettability measurements of MSN and CMSN drug-carrier preparations were also conducted to evaluate the functionality of carriers by using nimesulide (NMS) as a model drug. Drug loading samples composed of NMS and MSN or CMSN were prepared through solvent deposition method at the drug:carrier ratio of 1:2 (w/w), and denoted as NMS-MSN and NMS-CMSN, respectively. Drug loading content (%) was determined by taking an accurately weighed quantity of NMS-MSN and NMS-CMSN, extracting the loaded drug completely using NaOH solution (0.1 mol/L) under ultrasound, and measuring the drug content by using

ultraviolet (UV) spectroscopy (UV-1750, Shimadzu, Japan) at the wavelength of 394 nm. The initial contact angles of NMS, NMS-MSN, and NMS-CMSN were acquired using the same procedure of MSN and CMSN except that SIF was used to wet the tablet instead of water.

In vitro Degradation Study

To study the stability and degradation tendency of carriers, MSN and CMSN were precisely weighed, sealed, and incubated in SGF, SIF and SBF, respectively, with gentle shaking (150 rpm) at 37°C. Every week (7 days), the samples were taken out, separated by centrifugation, washed to remove the adsorbed degradation product and salts, dried, and precisely weighed. Then fresh degradation medium was added and the biodegradation procedures were repeated until all samples were thoroughly degraded.

The quantitative measurement of degradation was acquired by a gravity method, and the weight loss of samples was calculated as:

$$\text{Weight Loss}(100\%) = \frac{W_0 - W_t}{W_0} \times 100 \quad (1)$$

Where W_0 is the initial weight of carriers and W_t is weight of residual samples at the determined time t .

The degradation measurement was performed in triplicate.

Bio-Adhesion Study

All the experiments were approved by the Animal Ethics Committee of China Medical University. Animals were maintained in accordance with the guidelines for the Care and Use of Laboratory Animals. The bio-adhesion study of MSN and CMSN was performed by using an elution method. Sprague-Dawley (SD) rats weighing 180–220 g were fasted overnight with free access to water and sacrificed to separate the stomach and small intestine tissues. Then the stomach and small intestine tissues were carefully washed with normal saline (the mucous layer remained), respectively cut into pieces of 2 cm×2 cm and 2 cm×3 cm, and placed on a glass slide which was at a 45-degree angle from the horizontal platform. Then 20 mg MSN and CMSN were respectively evenly spread on the prepared, freshly excised tissue samples and wetted by a small amount of normal saline. After that, MSN and CMSN were allowed to eluate from the ex-vivo stomach and small intestine tissues by SGF, and SIF, respectively, by using a peristaltic pump at the flow rate of

2 mL/min (the schematic of the apparatus was shown in Figure 1D). Every 1 min, the effluent was collected, centrifuged to separate the residues, washed, dried, and weighed to quantify the bio-adhesion ability of carriers. The measurements were carried out in triplicate, and the bio-adhesion ratio was calculated by weight loss according to the following equation:

$$\text{Bio - adhesion ratio}(100\%) = \frac{W_0 - \sum_{i=1}^5 W_i}{W_0} \times 100 \quad (2)$$

Where W_0 is the initial weight of silica carrier, W_i is the weight of collected effluent at the determined time t .

In addition, the bio-adhesion of NMS, NMS-MSN, and NMS-CMSN were also assessed to evaluate the functionality of carriers in improving the bio-adhesive property of the drug. In this case, MMS (10 mg), NMS-MSN (containing 10 mg NMS), and NMS-CMSN (containing 10 mg NMS) samples were respectively exposed to the small intestine tissues. Then the elution procedure was conducted by using SIF as eluent at the flow rate of 2 mL/min, and every 1 min, the 2 mL effluent was collected. High performance liquid chromatography (HPLC) method was used to quantitatively analyze the drug content in effluent. The separation was performed on a Kromasil ODS-2 C₁₈ column (250 mm×4.6 mm) equipped with a JanuSep C₁₈ pre-column. UV visible detector was used for quantitative analysis with the absorbance value set at 370 nm. Mobile phase composed of 65% methanol and pH 7.3 35% potassium dihydrogen phosphate buffer (v/v) was used at a flow rate of 1 mL/min. The content of NMS was calculated by internal standard method.

Retention in the GI Tract Study

For ex vivo tracking, mesoporous silica nanoparticles were labeled with a fluorescent carbon quantum dots (PCA) tag and denoted as P-MSN and P-CMSN, respectively. Firstly, 0.6 g PEI and 0.6 g CA were dissolved in 10 mL distilled water, and stirred at 180°C for 2 h.²⁴ After that, the obtained bright yellow solution was separated by centrifugation at 16,000 rpm for 5 min, and then further purification by dialysis experiment (MWCO 3500 Da) for 48 h. The final brown product named PCA was obtained by freeze drying and the successful synthesized of PCA were verified using FTIR analysis. P-MSN and P-CMSN were respectively prepared by dispersing 10 mg MSN and CMSN into 1 mL PCA solution (10 mg/mL) and stirred for 2 h at room temperature. Finally, the resulting P-MSN and P-CMSN were

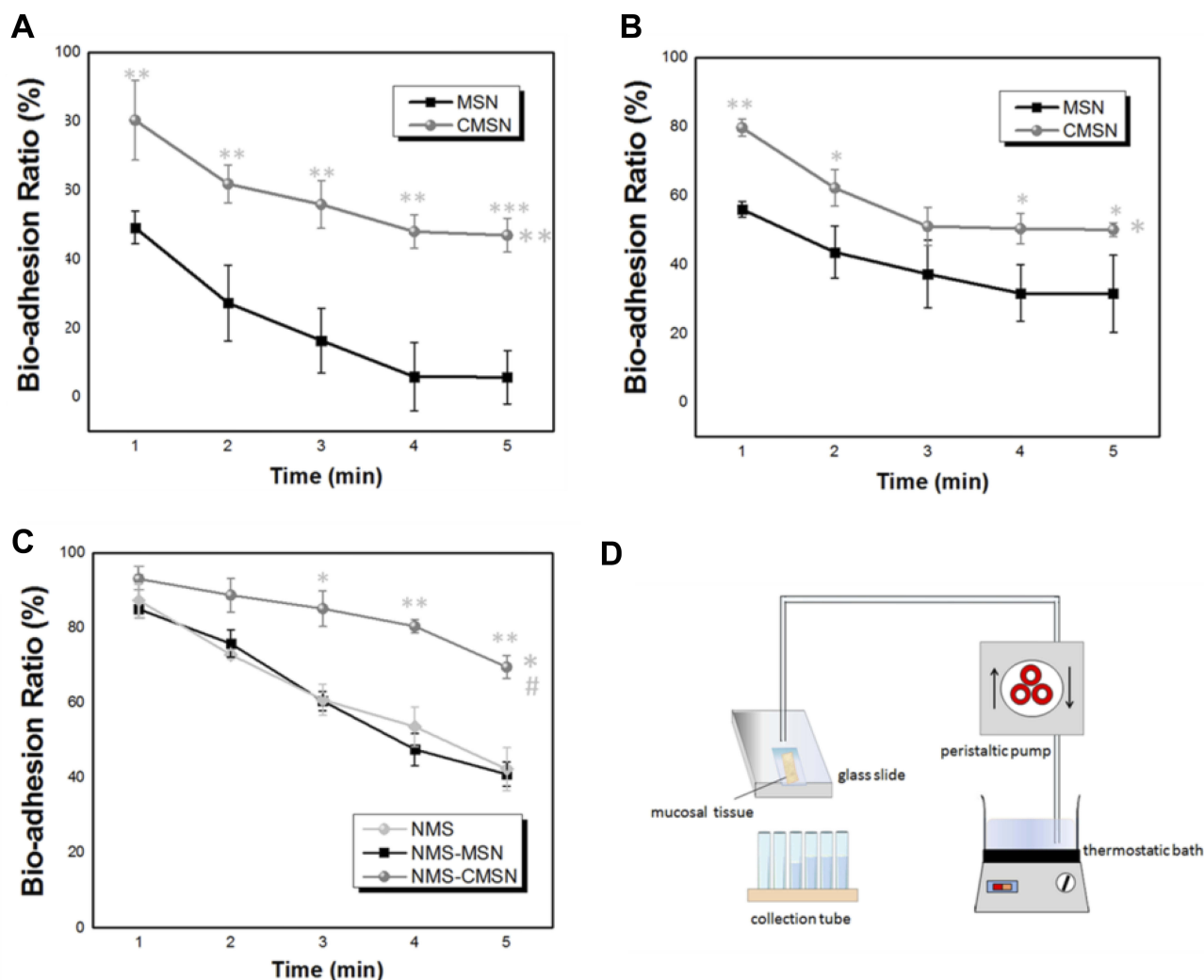


Figure 1 (A) Bio-adhesion profiles of silica carriers on small intestine tissues; (B) bio-adhesion profiles of silica carriers on stomach tissues; (C) bio-adhesion profiles of NMS, NMS-MSN and NMS-CMSN on small intestine tissues; (D) schematic illustration of the apparatus employed in the bio-adhesiveness study. * $P < 0.05$, ** $P < 0.01$, *** $P < 0.001$ compared to MSN; # $P < 0.05$ compared to NMS.

recovered by centrifugation, washed with water several times, and dried.

The GI tract retention ability of MSN and CMSN after oral administration was investigated using ex vivo imaging technology. 36 SPF-grade Kunming mice weighing 18–22 g were randomly divided into 2 groups ($n=18$ per group, $n=3$ at each time point): MSN group and CMSN group, and fasted overnight with free access to water before the experiment. Then P-MSN (2 mg) and P-CMSN (2 mg) suspended in 0.5 mL normal saline were intragastrically administrated to animals. At different time intervals of 0.5 h, 1 h, 2 h, 4 h, 8 h, and 12 h, animals were sacrificed, and the entire GI tract, including stomach, small intestine, and large intestine were excised. Fluorescent images were collected using IVIS Lumina Series III Living Image system (Caliper Life Sciences, USA) equipped with an

excitation filter of 410 nm and an emission filter of 535 nm. Region-of-interest values were captured as photon flux in total photon count per cm^2 per steradian.

Hemolysis Assay

In order to evaluate the blood compatibility of CMSN, hemolysis assay was carried out and compared with MSN. Fresh rabbit blood sample was collected via the marginal ear vein, and residual red blood cells (RBCs) were obtained by centrifugation, and washed with sterile isotonic saline. Then RBCs were diluted to a concentration of 2% (v/v) solution by sterile isotonic saline and were respectively added to an equal volume of sterile isotonic saline containing silica carriers ranging from 400 to 1600 $\mu\text{g}/\text{mL}$. Meanwhile, sterile distilled water and pure sterile isotonic saline were also used to prepare 2% RBCs

solution and served as positive control and negative control, respectively. After shaking for 4 h, the liquid supernatant was carefully collected. The images of the liquid supernatants were photographed, and the absorbances of the liquid supernatants were measured by using ultraviolet spectroscopy at a wavelength of 541 nm. The hemolysis percentages (%) of carriers were calculated using the following equation:

$$\text{Hemolysis percentage (\%)} = \left(\frac{A_{\text{test}} - A_{\text{negativecontrol}}}{A_{\text{positivecontrol}} - A_{\text{negativecontrol}}} \right) \times 100 \quad (3)$$

The A_{test} means the absorbance value of the tested group, $A_{\text{negativecontrol}}$ and $A_{\text{positivecontrol}}$ are the absorbance value of negative group and positive group, respectively. The hemolysis tests were performed in triplicate and data were expressed as the mean \pm SD.

In vitro Toxicity of CMSN

Cell Lines and Cell Culture

HepG2 cells and HUVEC cells were purchased from the American Type Culture Collection (ATCC, China) and maintained according to the ATCC. The cytotoxicity test of CMSN was performed on HepG2 cells and HUVEC cells, respectively. HepG2 cells were maintained in DMEM containing 10% FBS, while HUVEC cells were cultured in RPMI medium supplemented with 10% FBS. All cell lines were incubated at 37°C in an atmosphere of 5% CO₂.

Cell Viability Assay

To determine the safety of L-tartaric modification, cell viabilities were appraised using MTT assay. Briefly, HUVEC cells and HepG2 cells in growth medium were seeded in 96-well plates for 24 h at a density of 10⁴ cells/well and 10⁵ cells/well, respectively. After removal of the medium, fresh medium containing CMSN ranging from 0.02 to 200 µg/mL was added and treated for 24 h. Then 20 µL 5 mg/mL MTT was added to each well and incubated for an additional 4 h. The medium was then replaced by 150 µL DMSO, and the absorbance of each well was read at the wavelength of 570 nm by using a microplate reader after shaking on the horizontal rotators.

Cell Cycle and Apoptosis Analysis

HepG2 cells were plated in 6-well plates at a density of 2×10⁵ cells/well. After incubating for 24 h, the medium was removed, and the wells were washed and treated with fresh medium containing CMSN ranging from 0 to 100 µg/

mL for 12 h. After trypsinization, cells were then harvested, fixed in 70% ethanol, stained with propidium iodide, and sent to the flow cytometer (Becton Dickinson, USA) to analyze the cell cycle and apoptosis.

In vivo Toxicity of CMSN

To further investigate the in vivo toxicity of CMSN, 12 SD rats (weighing 180–200 g) were randomly allocated to 2 groups (n=6 per group): Control group and CMSN group. CMSN suspension in 2 mL normal saline at a dose of 200 mg kg⁻¹ was orally administrated to animals in CMSN group once a day for 28 days. The control group was given an equal volume of normal saline once a day. Animals were given a standard rodent diet, and body weight and clinic manifestation were recorded. 2 days after the last administration, animals were fasted overnight, and blood samples were drawn from aorta abdominalis to analyze the hematological (COBAS INTEGRA 800, Roche, Germany) and biochemical parameters (pocH-100i, SYSMEX, Japan). In detail, hematological parameters were analyzed using the whole blood, and biochemical parameters were obtained using the serum, which was separated from blood samples by centrifugation. After collection of blood samples, animals were sacrificed, and the main organs including the liver, heart, spleen, lungs and kidneys were recovered and weighed to calculate the ratio of tissues to body. Then the recovered tissues were fixed in 10% formalin, embedded in paraffin, sectioned, stained with hematoxylin and eosin (H&E), and examined by light microscopy.

Statistical Analysis

All data were expressed as the mean \pm SD. One-way ANOVA was applied to compare the control and test values. Student's *t*-test was employed to determine identify levels of significance between the groups. Statistical significance was set as *p*<0.05.

Results and Discussion

Characteristics of MSN and CMSN

By using the synthesized chiral silane coupling agent (APTRES), CMSN was synthesized via co-condensation method. Initially, CTAB self-assembled to form micelles in water. After addition of APTRES and TEOS, the positively charged head groups of the CTAB electrostatically interacted with the negatively charged carboxyl groups of the APTRES. Meanwhile, owing to the existence of ammonia, the silica source TEOS presented negative

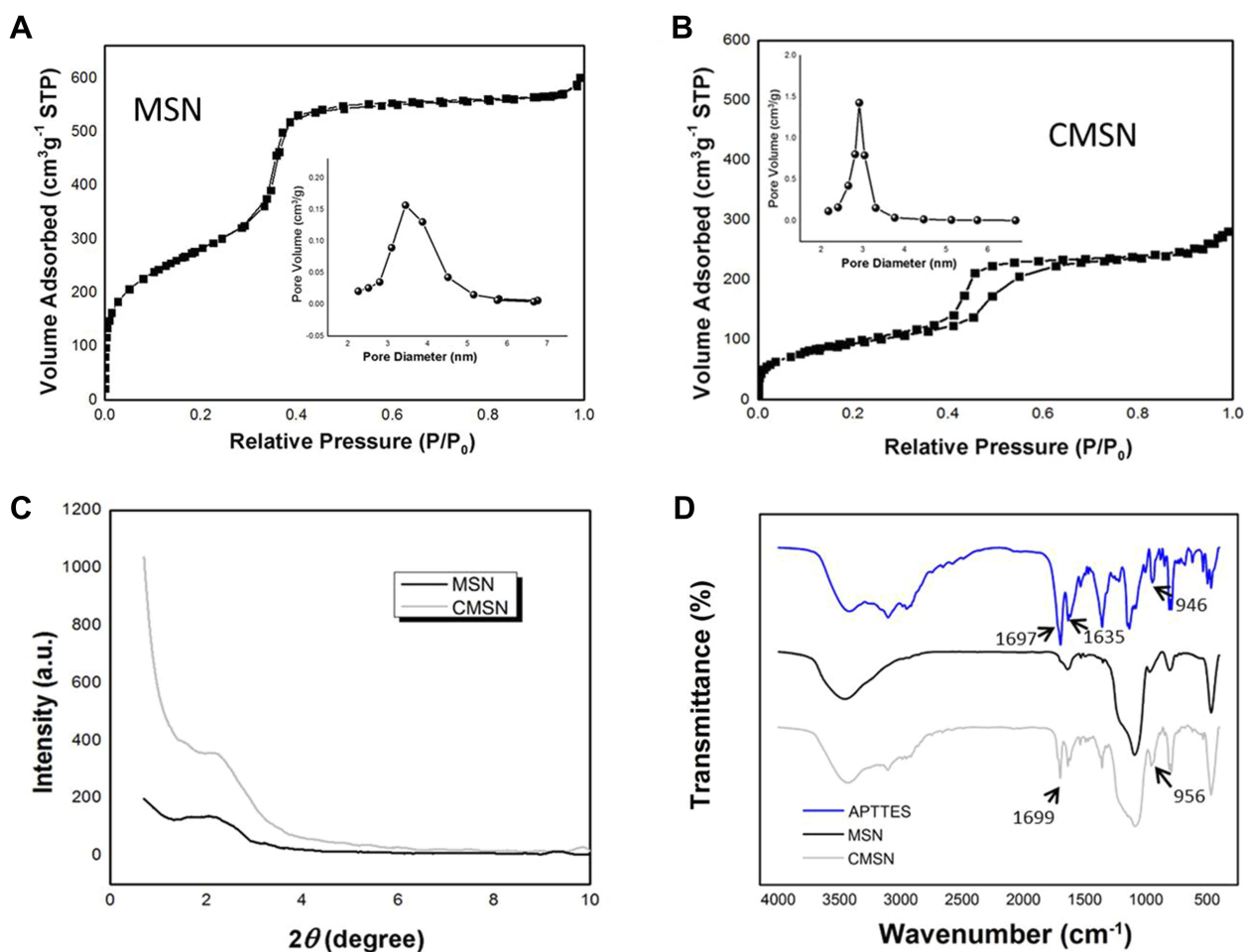


Figure 2 (A) Nitrogen adsorption/desorption isotherm and pore size distribution curve of MSN; (B) nitrogen adsorption/desorption isotherm and pore size distribution curve of CMSN; (C) SAXD patterns of MSN and CMSN. (D) FTIR spectra of APTES, MSN, and CMSN.

charge under alkaline condition, and CTAB also electrostatically interacted with the negatively charged silica hydroxyl groups hydrolyzed from TEOS. Interactions conducted on the organic/inorganic hybrid interface were categorized as the synthesis route of $M^+S^-I^-$, where M^+ stood for APTES with negative carboxyl groups, S^- represented cationic CTAB, and I^- stood for TEOS with negative charge.²² At the same time, the alkoxy silane sites of APTES polymerized with TEOS to form silica framework. Along with the deposition of silica precursor, chiral mesoscopic structure was imprinted in CMSN.

Figure 2D showed the FTIR spectra of APTES, MSN and CMSN. In the FTIR spectra of APTES, the presence of amide linkages (-CONH-) was evidenced by the carbonyl group stretching vibration of amide at 1634.7 cm^{-1} , indicating that APTES was successfully linked with L-tartaric acid. The stretching band of carboxylic acid was found at 1697.0 cm^{-1} , and the stretching and out-of-plane bending

vibrations of -OH group were observed at 3422.0 cm^{-1} and 946.1 cm^{-1} , respectively. The results proved that only one carboxyl group of L-tartaric acid functioned with amino group of APTES, and the unbounded carboxyl group can be used to conduct carboxylic modification. As for MSN and CMSN, the Si-O-Si bending vibrations were respectively shown at 466.9 cm^{-1} and 467.6 cm^{-1} , and the Si-O-Si antisymmetric stretching vibrations were respectively located at 1094.7 cm^{-1} and 1085.5 cm^{-1} , which were all characteristic bands of silica materials. Especially, the 1699.3 cm^{-1} and out-of-plane bending vibration of carboxylic hydroxyl at 956.4 cm^{-1} which appeared in the FTIR spectra of CMSN strongly confirm the successful grafting of L-tartaric acid.

As the most authoritative testing method, CD apparatus was applied to characterize and elucidate the chiral structure of CMSN. The presence of erected peak at the wavelength of 219 nm proved the chirality of CMSN (Figure 3H), while

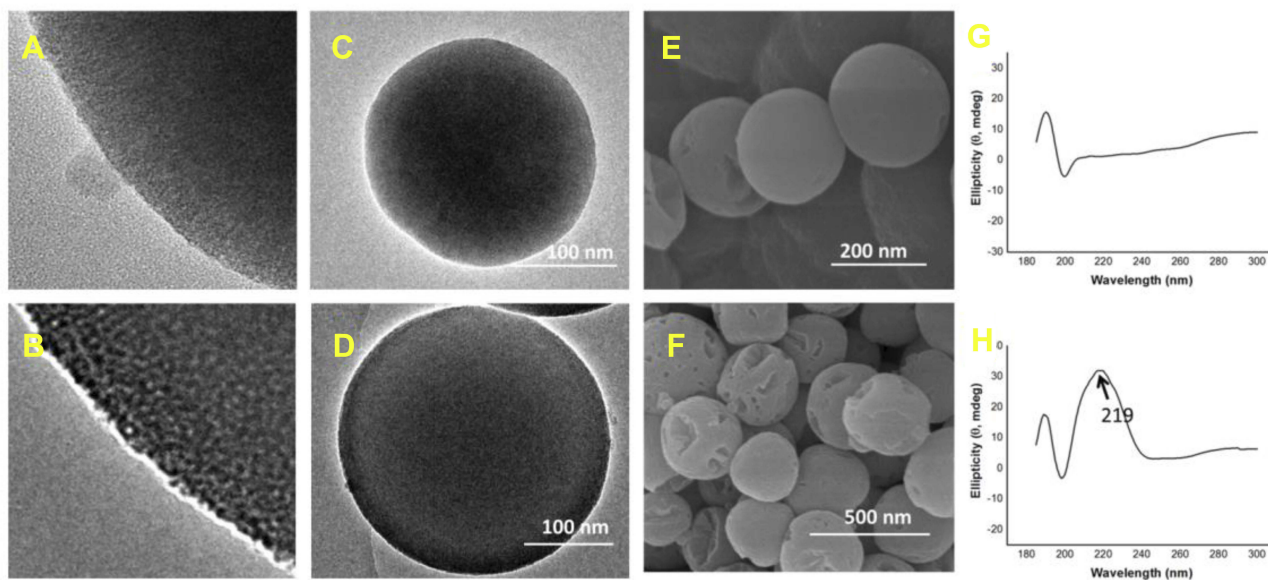


Figure 3 Structural characteristics of MSN and CMSN. (A) Amplifying TEM images of MSN; (B) amplifying TEM images of MSN; (C) TEM images of MSN; (D) TEM images of MSN; (E) SEM image of MSN; (F) SEM image of CMSN; (G) CD spectra of MSN; (H) CD spectra of CMSN.

Note: The arrow in Figure 3 (H) indicated the main peak position of the CD spectra.

MSN (Figure 3G) failed to induce CD activity within the UV absorbance band of 210–300 nm, confirming the achiral nature.

The morphology and structure of silica carriers were measured by TEM and SEM. As indicated in Figure 3, both MSN and CMSN were well-formed spherical nanoparticles with mesopores, and the particle size of MSN and CMSN were 200 nm and 300 nm, respectively. In particular, the silica framework of MSN was more compact in the core than the shell of nanoparticles (Figure 3C), and some straight nanochannels were radially distributed on the shell (Figure 3A). While more distinguishable core-shell structure could be observed in the TEM image of CMSN (Figure 3D) with a thin layer composed of a large number of honeycombed curved mesopores presenting at the edge of the nanospheres (Figure 3B). The silica framework of CMSN was more compact in the thin shell since the functional group of APTTES was longer than that of TEOS that resulting in slower condensation rate.

The nitrogen adsorption–desorption isotherms and pore size distribution curves of MSN and CMSN were shown in Figure 2. Both MSN and CMSN possessed typical type IV isotherms with capillary condensation steps, suggesting the existence of uniform mesopores. The textural parameters were displayed in Table 1, and the S_{BET} , V_t and D_{BJH} of MSN were 805.82 m^2/g , 0.75 cm^3/g , and 3.37 nm, respectively. After

surface modification with L-tartaric acid, the S_{BET} , V_t and D_{BJH} of CMSN were respectively reduced to 418.27 m^2 , 0.41 cm^3/g , and 2.97 nm, due to the large number of modified carboxyl groups, thus taking up a certain amount of nano-space. As can be seen in Figure 2C, the SAXD pattern of CMSN and MSN showed the main peak at 2.2° (2θ), implying the successful forming of mesostructure. Compared to MSN, the main peak of CMSN had increased intensity, demonstrating that the order degree of mesostructure was increased after grafting L-tartaric acid onto silica framework using APTTES.

Wettability

Wettability, an extremely important interfacial property, was closely associated with the in vitro and in vivo functionality of bio-materials.^{25–27} As kinds of potential drug carriers, the wettability of MSN and CMSN was studied. According to Figure 4A, the initial contact angle values of MSN and CMSN were $35.43 \pm 2.12^\circ$ and $27.35 \pm 1.02^\circ$, respectively, indicating good wettability. Besides, the contact angles of

Table 1 Specific Surface Area, Pore Volume, Pore Diameter and Drug Loading Content of Silica Carriers

Sample	S_{BET} (m^2/g)	V_t (cm^3/g)	W_{BJH} (nm)	Drug Loading Content (%)
MSN	805.82	0.75	3.37	26.12 ± 0.95
CMSN	418.27	0.41	2.97	28.55 ± 1.27

MSN and CMSN both decreased with time due to the porous nature of materials, and the equilibrium contact angles were reduced to $22.79 \pm 1.52^\circ$ and $15.34 \pm 1.64^\circ$, respectively (Figure 4B), due to the fact that the enriched pore structures enabled them to adsorb the water molecules from humid surroundings. The contact angles of CMSN were obviously lower than MSN, demonstrating the higher hydrophilicity, which was largely on account of the modified polar carboxyl groups. During the wetting process, the carboxyl groups on the surface of CMSN actively participated in the forming of hydrogen bonding with water and improved the hydrophilicity of CMSN. On the other hand, the wettability of materials was also governed by the surface geometrical microstructure.^{19,28} Concretely, on the surface of CMSN, polar functional groups (silanol group and carboxyl group) were distributed more compactly, because the smaller

nanochannels contributed to higher density of functional groups. And the stronger capillary condensation occurred in the smaller nanopores of CMSN which led to higher additional pressure, thus benefiting the wetting process (the mechanism was indicated in Figure 4D). It was clear that, after surface modification with L-tartaric acid, the wettability of silica carrier was largely improved.

By using nimesulide as a model drug, the wettability of the silica-drug formulations was estimated. According to Table 1, NMS could be loaded into MSN and CMSN with high efficiency. Notably, the higher drug loading capacity of CMSN could be attributed to the strong hydrogen bonding force formed between drug and surface modified carrier.²² As shown in Figure 4C, the initial contact angle of pure NMS was $69.11 \pm 4.28^\circ$ as a result of the poor hydrophilicity. After loading into MSN and CMSN, however, the initial

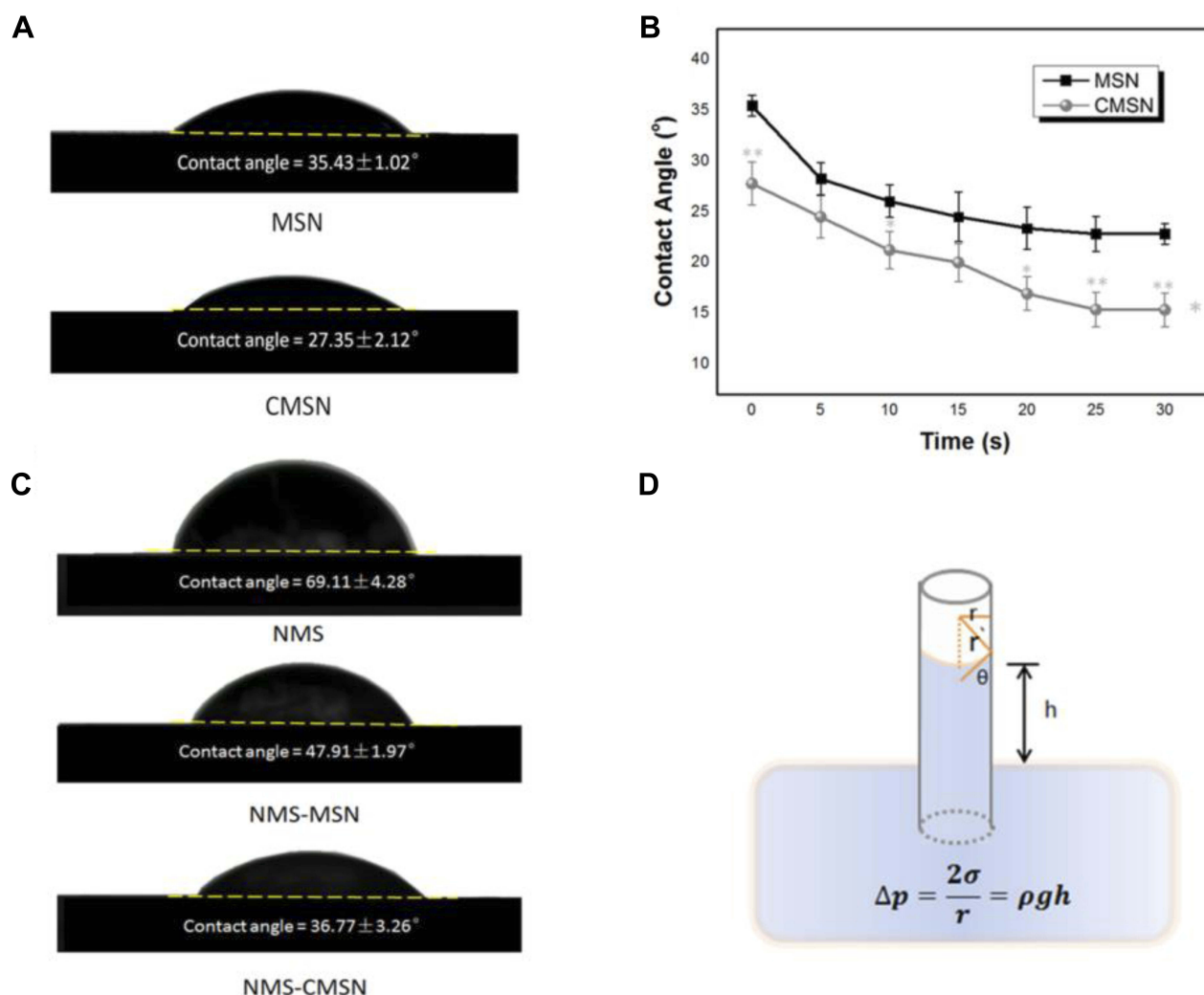


Figure 4 (A) Initial contact angles of silica carriers; (B) contact angles measured at different times and the equilibrium contact angles of silica carriers; (C) initial contact angles of NMS, NMS-MSN and NMS-CMSN; (D) schematic illustration of the capillary effect occurring in the mesopores of silica carriers. *P < 0.05, **P < 0.01 compared to MSN.

contact angle was significantly decreased to $47.91 \pm 1.97^\circ$ and $36.77 \pm 3.26^\circ$, respectively. Both MSN and CMSN could effectively enhance the wettability of hydrophobic drug, which was conducive for their *in vivo* absorption. Compared to MSN, CMSN exhibited much better ability in improving the wettability of drugs, and the result was in accordance with the wettability of silica carrier.

In vitro Degradation

In vitro degradation study of MSN and CMSN was respectively performed in SGF, SIF and SBF. These two silica carriers could dissolve thoroughly in simulated physiological fluids during a degradation period of 1–12 weeks (Figure 5). MSN and CMSN showed similar degradation tendencies in physiological fluids without statistical difference, which were mild degradation processes without any well-defined steps (the accumulative dissolvability was less than 20% in the first 1 week) in SGF and SBF, and

conspicuous mass loss in SIF (the degradation percentages were $80.10 \pm 5.37\%$ and $99.20 \pm 4.54\%$ within 1 week). The bulk degradation of mesoporous silica nanoparticles in SIF could be ascribed to the dissolution and ionic corrosion of the amorphous silica matrices formed by the hydrolysis and condensation of silica source.^{19,29}

As a kind of interface reaction, it was thought that the surface reaction barrier in the degradation process can be effectively reduced by large surface area and large pore size.^{29,30} Interestingly, compared to MSN, CMSN with smaller pore size and surface area possessed faster degradation rate in all three kinds of simulated body fluids, which was exactly the opposite of the previous studies. It dissolved thoroughly (weight loss >99%) within 8, 1, and 11 weeks in SGF, SIF, and SBF, respectively. Meanwhile, MSN took 11, 2, and 12 weeks to degrade. According to the Young-Laplace equation, the smaller the contact angle, the higher the additional pressure (as shown in Figure 5D).

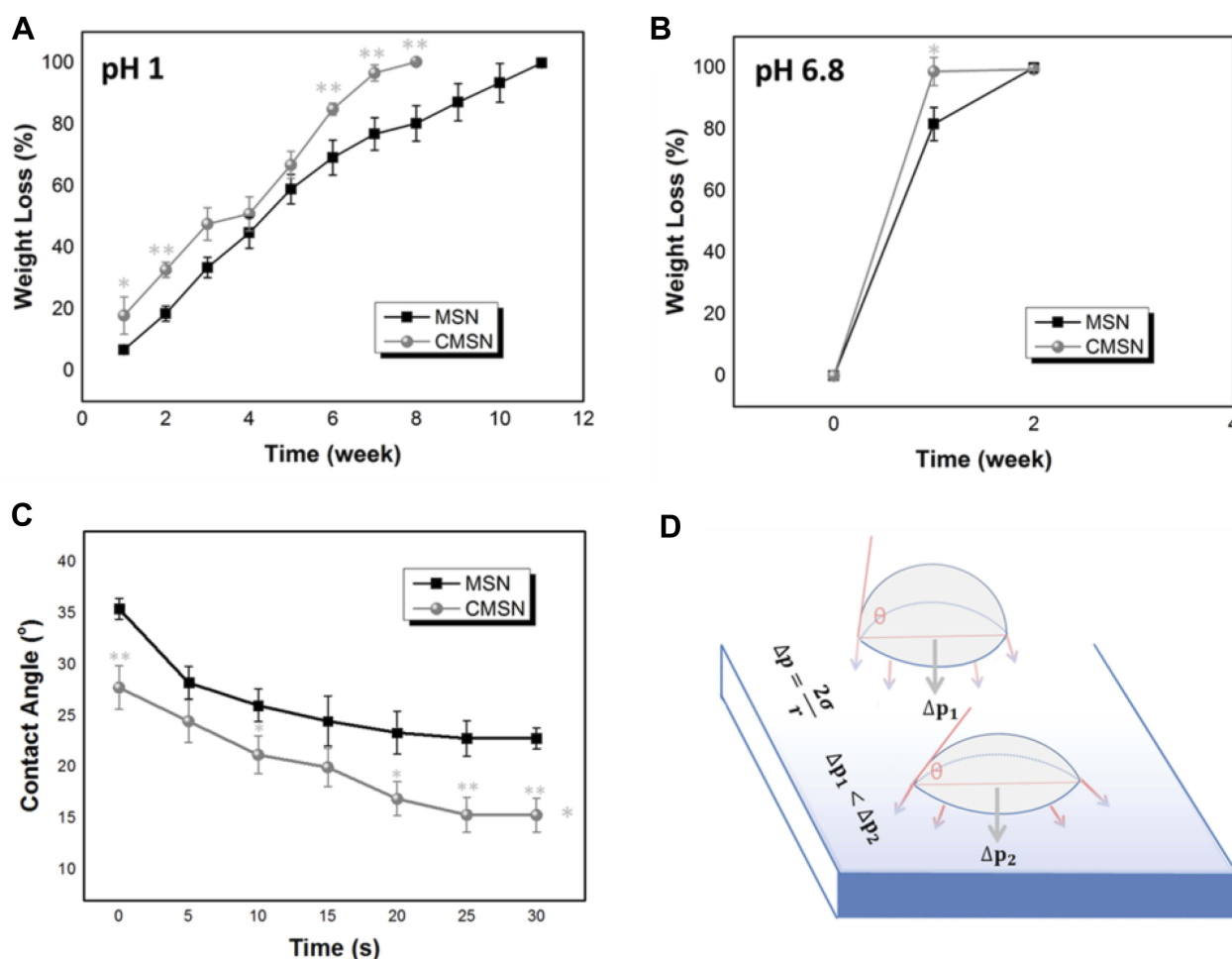


Figure 5 Degradation profiles of silica carriers in SGF (A), SIF (B) and SBF (C), and the schematic illustration of the additional pressure induced by carriers with different contact angles (D). *P < 0.05, **P < 0.01 compared to MSN.

The larger additional pressure in the smaller nanochannels of CMSN effectively “pulled” the degradation medium to enter the inner surface of pore channels, and the higher density of functional groups (silanol group and carboxyl group) led to stronger hydrogen bonding force, which promoted the dissolution of silica nanoparticle. Other than the structural properties, the degradation behavior of carriers was also influenced by the interface characteristics. Wettability, as an interface characteristic, had been proven to be vital for solid carriers by affecting their affinity with the liquid interfaces. The better wettability of CMSN meant a larger contact area, contributing to a higher possibility of interaction and a more rapid substance transfer.

Bio-Adhesion

Oral administration is a preferred delivery pathway for most therapeutic drugs since it has fewer safety concerns and the best patient compliance.^{31,32} However, challenges for oral delivery still exist, especially for drugs with low solubility, weak stability and poor permeability across epithelial tissue in the GI tract.³² Previous studies have indicated that by using CMSN and MSN as drug carrier, the solubility and stability of drug were improved because the crystallization of drug effectively changed to amorphous form in the confined rigid silica nanochannels.^{22,23} In this study, the bio-adhesion study was carried out on small intestine mucosa due to the fact that adhesion on the epithelial tissues was the prerequisite for drug absorption. According to the bio-adhesion profiles shown in Figure 3A, under mild downward liquid, the bio-adhesion ratios of MSN and CMSN were 49.12±8.72% and 80.29±11.61% at 1 min and 5.70±5.14% and 46.89±7.88% at 5 min, respectively. The bio-adhesion ability of CMSN was remarkably higher than MSN ($P=0.008$ at 1 min, $P=0.0006$ at 5 min) owing to the higher wettability and additional pressure, which meant higher probability for the uptake of carrier or the passive absorption of the guest drug. Aside from this main recognized reason, the molecular chiral topographical structure on the surface of CMSN also produced higher friction when coming into contact with mucosa tissue. Besides, the bio-adhesion study on gastric mucosa was also conducted, and the results (the bio-adhesion ratios were 56.03±3.21% and 79.72±4.38% at 1 min, 31.54±11.13% and 51.72±2.05% at 5 min for MSN and CMSN, respectively, Figure 3B) also indicated higher mucosa-adhesion ability of CMSN. It can be concluded that L-tartaric acid modification had

improved the mucosa-adhesion ability of drug carrier, which would be vital for their final destiny in vivo.

The potential of silica carriers to improve the bio-adhesion of therapeutic drug was also explored by using nimesulide as a model drug, and the results were shown in Figure 3C. The bio-adhesion ratios of NMS, NMS-MSN and NMS-CMSN were 87.30±5.55%, 84.91±2.26% and 93.02±4.23% at 1 min, 42.28±3.01%, 40.91±3.21% and 69.64±2.72% at 5 min, respectively. Compared to pure NMS, there was no significant difference between NMS and NMS-MSN. However, NMS-CMSN possessed higher mucosa-adhesion ability, which was of great importance to achieve efficient drug delivery. Furthermore, the variations of all bio-adhesion ratios with time were analyzed, and the bio-adhesion-time curves of CMSN showed significant statistical difference compared to MSN and NMS. Herein, both chiral topographical structure and functional groups had strong impact on the biological properties of silica carriers.

Retention in the GI Tract

On the basis of the results mentioned previously, it could be reasonably speculated that CMSN remained in the GI tract for a longer time. To verify this hypothesis, MSN and CMSN were labeled with a fluorescent tag (PCA), and the retention behavior was investigated and visualized using ex image technology. The successful synthesis of PCA was verified using FTIR (Figure 6B), the stretching vibration and bending vibration of -NH were respectively noticed at 3422.5 cm^{-1} and 1563.8 cm^{-1} , and the vibrational absorption bands of -C=O were found around 1650.3 cm^{-1} . The characteristic absorptions assigned to -CONH- groups dominated the tight connection of PEI and the quantum dots formed by CA. As can be seen in Figure 6A, at 0.5 h post administration, most of the fluorescence signal was captured in the stomach. After an initial increase in fluorescence, the fluorescence intensity in the MSN group decreased quickly after 1 h (Figure 6C). For CMSN, the fluorescence intensity in the GI tract increased with time and peaked at 2 h post administration because of the higher adhesive force in the stomach, and then the fluorescence signal weakened gently. Even after 12 h, the fluorescence intensity of CMSN remained at a higher level ($P=0.009$), due to the stronger mucosa-adhesion ability and the higher friction in stomach and small intestine. It should be noted that the fluorescence in stomach decreased over time for MSN, while CMSN accumulated in the stomach since the stronger adhesive force slowed

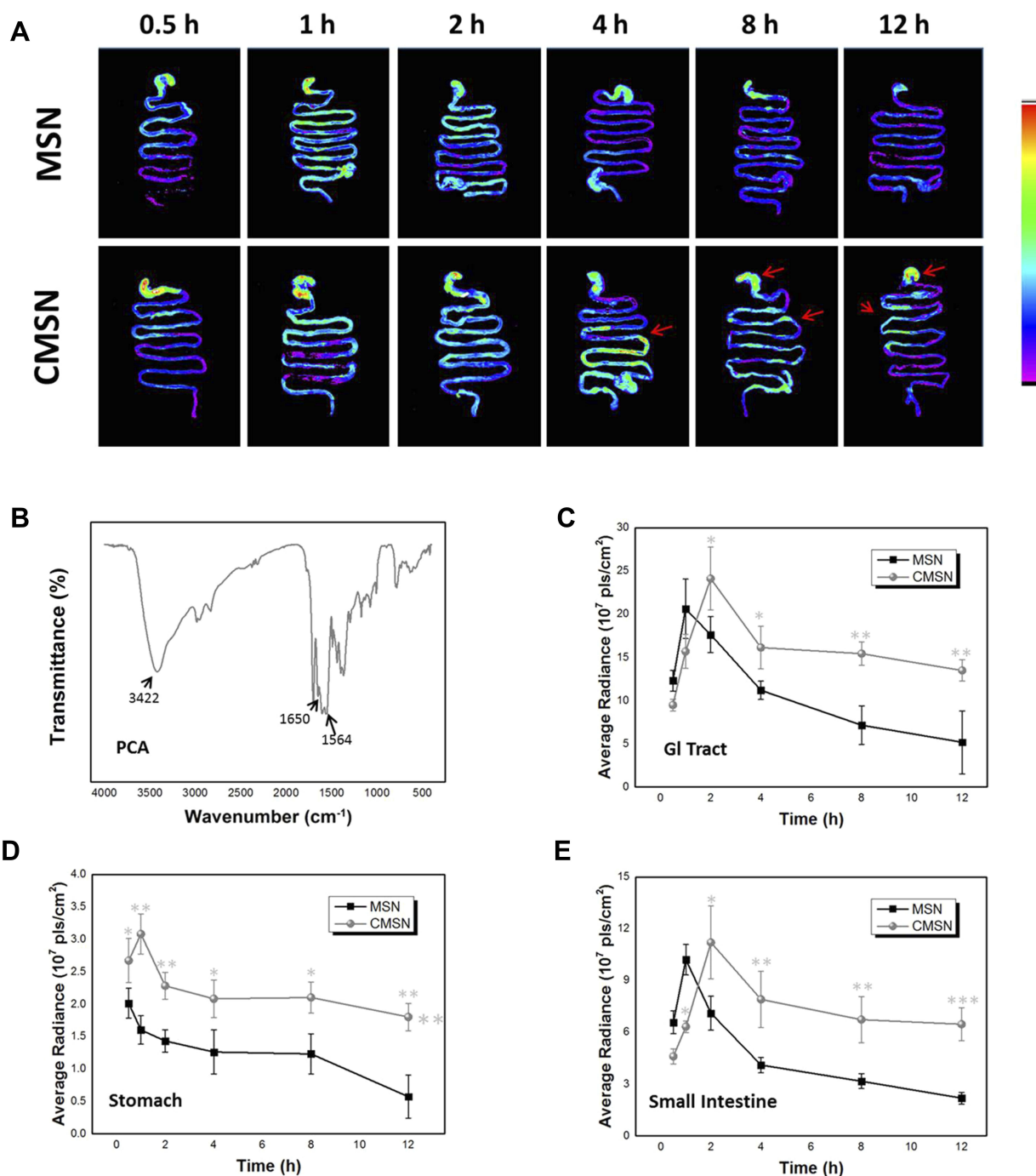


Figure 6 (A) Photographic images of silica carriers which remained in the whole GI tract at different time intervals after oral administration; (B) FTIR spectra of PCA; (C) the accumulation of silica carriers in GI tract at different times; (D) the accumulation of silica carriers in stomach at different times; (E) the accumulation of silica carriers in small intestine at different times. * $P < 0.05$, ** $P < 0.01$, *** $P < 0.001$ compared to MSN.

down the gastric emptying (Figure 6D). Moreover, according to Figure 6E, the fluorescence signal of MSN in small intestine, that served as a major organ of digestion and absorption, started to decline at 2 h post administration, and little fluorescence could be detected in the small intestine after 4 h. In contrast, a considerable amount of

the CMSN was stranded in the jejunum and ileum at 12 h ($P=0.0008$), and was favored for the passive absorption of the cargo. These findings demonstrated that CMSN had stronger retention ability in the GI tract, which was crucial for the final destiny of drug carrier and can advantageously affect the absorption of the guest biomolecules or drugs.

Hemocompatibility

Blood compatibility was one of the most important concerns regarding the safety of biomaterials, since nanocarriers have a certain probability to enter into the blood stream no matter what administration route was adopted. For silica-based materials, the hemolytic effect which might cause irreversible damage to erythrocytes was thought to be triggered by the reactive oxygen species (ROS) on the surface of the carrier, the high affinity between the tetraalkylammonium groups in the membranes of erythrocytes and silica, and the electrostatic interactions between the membrane proteins and silica.^{16,39} The blood compatibility of MSN and CMSN was estimated by hemolysis assay, and the

results were displayed in Figure 7A and B. For CMSN, very low hemolysis of rabbit erythrocytes was observed at the concentration of 100–400 $\mu\text{g/mL}$. Even at the concentration of 800 $\mu\text{g/mL}$, which was an excessive value for drug delivery and high enough for other biological applications, the hemolysis ratio of CMSN was below 5% ($4.86 \pm 0.76\%$), suggesting that the CMSN would not lead to severe hemolysis according to ISO 10993-4:2002.⁴⁰ Nonetheless, for MSN, the hemolysis ratio was higher than 5% when the concentration was larger than 400 $\mu\text{g/mL}$. To the best of our knowledge, the negatively charged carboxyl groups might have had an adverse effect on the blood compatibility of CMSN, because the electrostatic

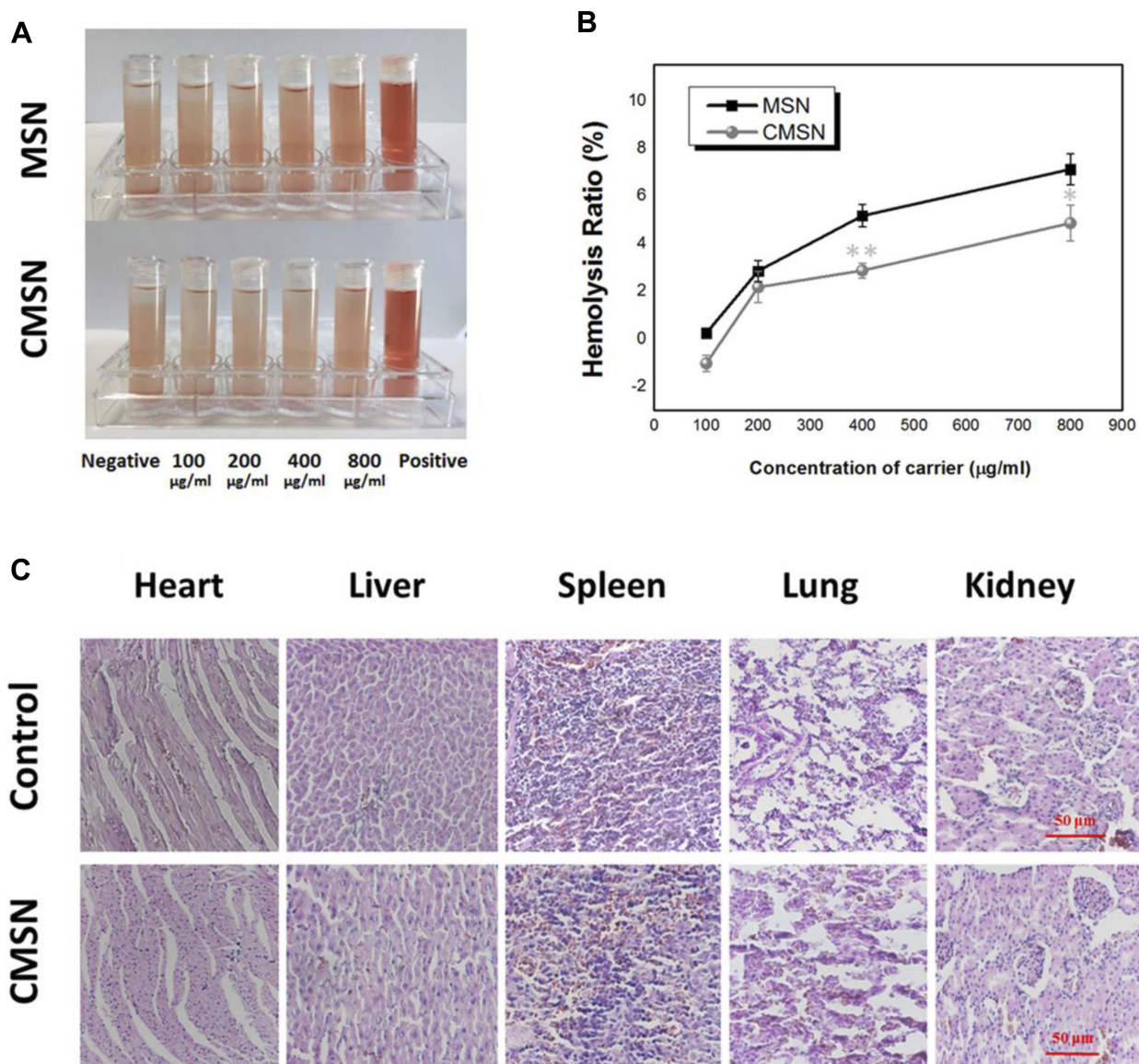


Figure 7 (A) Hemolytic photographs of silica carriers; (B) hemolysis ratios of silica carriers; (C) effect of CMSN on the main organs of rats. * $P < 0.05$, ** $P < 0.01$ compared to MSN.

interactions between silica and erythrocytes membrane were related to the zeta potential of silica.⁴⁰ In this case, the hemocompatibility of CMSN with negative charge was better than that of MSN. Apart from the surface charge, the hemolysis of materials was also influenced by the hydrophilicity, and the grafted polar carboxyl groups of CMSN enhanced the hydrophilicity (as indicated by the contact angles) and could shield the ROS on the surface. Therefore, CMSN exhibited good hemocompatibility, and had no destructive effect on erythrocytes when circulating in the blood.

In vitro Toxicity

Numerous studies have demonstrated that most naked silica-based drug carriers were inorganic nanomaterials with good biocompatibility, and the biocompatibility was affected by the physicochemical parameters, such as surface property, size, shape, and mesoscopic structure.^{6,18,19,33,34} For surface functionalized MSNs, their properties were also determined by the composition of nanoparticles and the type of functional groups.^{6,35–37} Along with a wide range of biomedical applications, surface functionalized mesoporous silica nanoparticles were thought to be biocompatible, and that they should be able to integrate with a biological system without causing cellular toxicity, genotoxicity, hemolytic reaction, inflammation or immune rejection. So, the biocompatibility and toxicity of CMSN were studied both in vitro and in vivo to evaluate the safety of L-tartaric acid modification.

Cytotoxicity test of CMSN was performed on HepG2 cells and HUVEC cells at a dose of 0.02–200 $\mu\text{g/mL}$ by using MTT assay. As shown in Figure 8A, after 24 h of incubation, the HepG2 cell viability remained higher than 88% within the tested range, even after incubation with higher CMSN concentration (200 $\mu\text{g/mL}$), the cell viability remained at a high level, and the cell viability was not reduced with increasing CMSN concentration. Besides, CMSN also showed negligible cytotoxicity to HUVEC cells (Figure 8B), and the cell viability remained higher than 85% within the tested range. The results suggested that CMSN did not produce significant cytotoxicity even at higher concentrations, which indicated excellent biocompatibility.

Cell cycle and apoptosis analysis was also conducted, as cell cycle arrest and cell apoptosis were considered as two major events of cell growth inhibition.^{21,38} The cell cycle distribution of HepG2 cells was analyzed by flow cytometer after incubation with CMSN at a dose of 0–100

$\mu\text{g/mL}$. As revealed in Figure 8C, the cell cycle distribution of the treated groups was similar to the untreated samples. There was no significant difference between the treated groups with different CMSN exposure doses, and the cell cycle distribution did not show any dose-dependent. In addition, no sub-G1 population was observed, demonstrating no obvious cell apoptosis induced by CMSN. The results indicated that CMSN did not block the cell cycle, inhibit the cell growth or arouse cell apoptosis.

In vivo Toxicity

To detect the underlying in vivo toxicity of CMSN to animals, it was orally administered to animals once a day for 28 days at a dose of 200 mg/kg. During the entire study period, bodyweight, clinical manifestations and histopathology of animals were recorded. Under strict medical observation, no sudden animal death, obvious abnormal symptoms or severe side effects were noticed. CMSN showed no suppression of weight gain, the mice in the control group and CMSN treated group respectively gained 15.19 \pm 1.63% and 16.60 \pm 1.04% body weight. Moreover, the major organs including heart, liver, spleen, lung and kidney were collected from animals in control group and CMSN group, all organs were normal in shape without inflammation, hypertrophy or necrosis; all coefficient indices were within the reference ranges and the two groups had no statistical differences (data not shown). To further assess the tissue toxicity of CMSN on a microscopic level, major organs were subject to histological evaluation. As can be seen in Figure 7C, all H&E stained tissue slices showed no evident histological abnormality such as structural change, appreciable lesion, damage, or inflammation, indicated no tissue toxicity of CMSN.

Systemic effects of CMSN were studied by measuring hematological and serum biochemical markers of animals after the 28 days continuous administration. It was well known that the entrance of immunogenic potential particulate materials, degradation products or residual surfactant into the systemic circulation might induce severe inflammatory reaction or cause anomalies in related hematology indicators.^{33,41} Various hematology parameters including leukocyte counts (WBC), red blood cell count (RBC), hematocrit (HCT), hemoglobin (HB), mean corpuscular hemoglobin (MCH), mean corpuscular volume (MCV), mean corpuscular hemoglobin concentration (MCHC), platelet counts (PLT), thrombocytocrit (PCT),

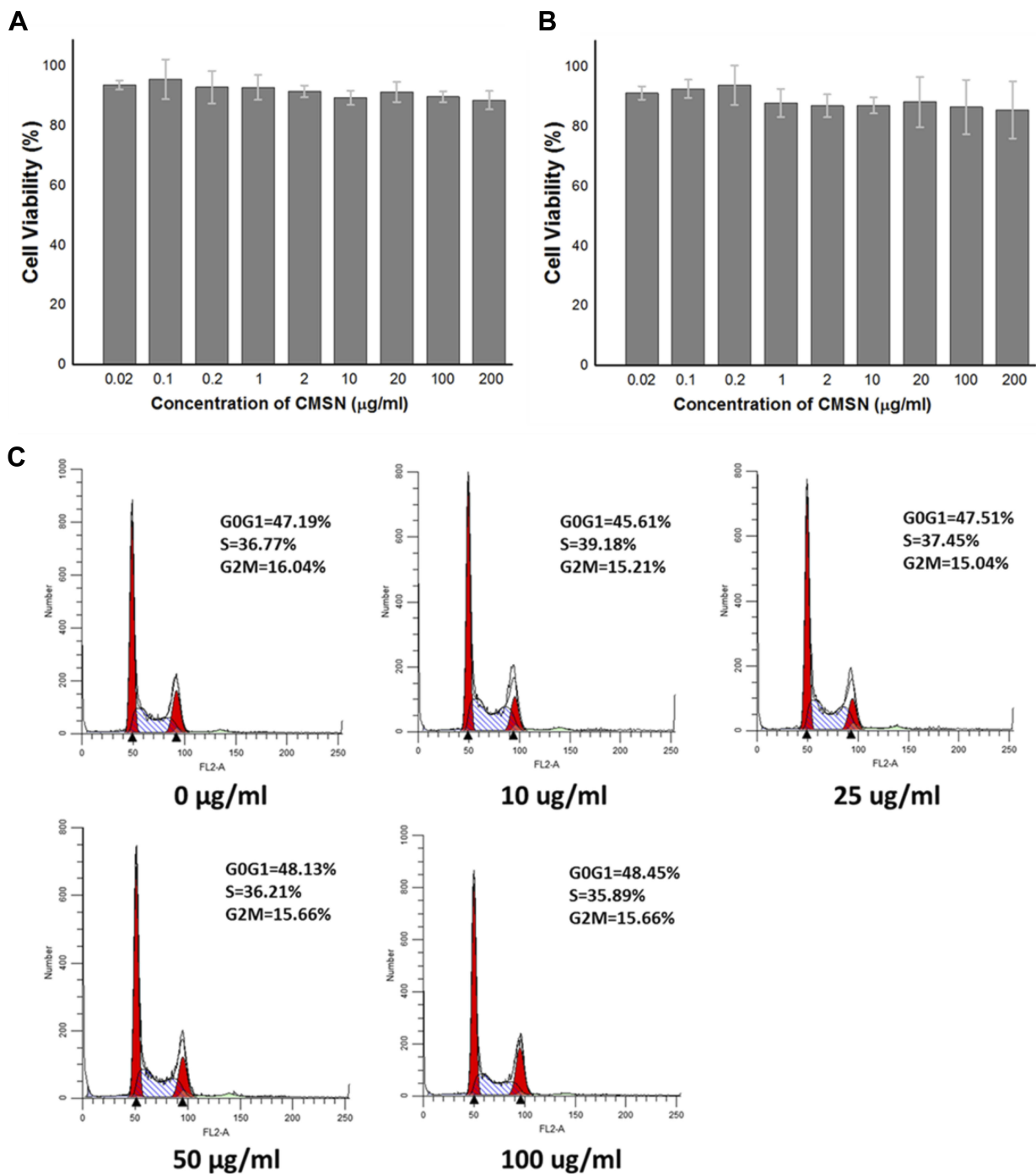


Figure 8 The effects of CMSN on viabilities of HepG2 cells (A) and HUVEC cells (B), and on cell cycle progression of HepG2 cells (C).

mean platelet volume (MPV), platelet distribution width (PDW), coefficient of variation of RBC volume distributing width (RDW-CV) and standard deviation of RBC volume distributing width (RDW-SD) were tested by assessing complete blood counts. For all the measured parameters, the results were within the normal ranges, and there was no significant change between the control

group and CMSN group (Table 2).^{33,42,43} This suggested no obvious hematological toxicity, and CMSN would not promote any adverse trend to the blood cells and components.

Moreover, it was crucial to measure the hepatic and renal functions after the continuous CMSN exposure, since liver and kidneys are the main place for metabolism and clearance

of exogenous substances.⁴¹ To evaluate the potential damage caused by CMSN, the representative serum biochemistry parameters were acquired, including the liver function indicators, such as alanine transaminase (ALT), aspartate transaminase (AST), alkaline phosphatase (ALP), total bilirubin (TBIL), indirect bilirubin (IBIL), direct bilirubin (DBIL), albumin (ALB), globulin (GLB), total protein (TP), the ratio of albumin and globulin (A/G); and the kidney markers, for example, the creatinine (CREA), blood urea nitrogen (BUN), and uric acid (UA). According to Table 3, almost no significant difference was detected in all biochemical parameters after administration of CMSN (except GLB and TP).^{18,42–44} The results indicated that CMSN did not promote severe abnormalities of the hepatic and renal functions, and was proven to be safe in vivo. Based on the in vitro and in vivo results, it was reasonable to speculate that CMSN was a biocompatible bio-material with negligible toxicity, and was suitable for further applications in biological fields.

Conclusion

In this study, CMSN with functions of carboxyl modification and chirality was synthesized through co-condensation method by using the chiral silane coupling agent APTES. The results

showed that CMSN and MSN were well-formed spherical nanoparticles with uniform mesoporous structure. As an extremely important interfacial property, the wettability of carriers was dependent on the structure characteristics and surface modification, CMSN with smaller pore size and carboxyl modification exhibited better hydrophilicity. The in vitro and in vivo behaviors of carriers, including degradation, bio-adhesion, and retention ability were largely related to the wettability of materials. Both CMSN and MSN could dissolve thoroughly in simulated physiological fluids during a degradation period of 1–12 weeks, and CMSN had faster degradation rate compared to MSN. Besides, CMSN possessed higher mucosa-adhesion ability in gastric mucosa and small intestinal mucosa, and also had the potential to improve the bio-adhesion of therapeutic drug. Particularly, CMSN had longer retention time in the GI tract compared to MSN, a considerable amount of CMSN was stranded in the small intestine at 12 h post administration, which meant higher probability for the uptake of carrier or the passive absorption of the drug substances. Finally, the biocompatibility and toxicity of CMSN was systematically estimated, and the results indicated that CMSN was a kind of biocompatible bio-material with good blood compatibility and negligible toxicity, which is beneficial for further biomedical applications.

Table 2 Effect of CMSN on Hematological Parameters of Rats

	WBC	RBC	Hb	Hct	MCV	MCH	MCHC
Control	12.8±7.8	6.7±1.6	149.8±5.3	38.1±9.8	57.1±2.5	20.3±0.4	357.3±13.9
CMSN	10.4±2.5	7.4±0.7	147.3±9.4	41.9±4.4	56.3±0.9	19.8±0.7	351.8±12.6
Reference	2.3–31.6	6.4–9.4	119.1–173.4	29.7–49.8	48.5–66.5	16.8–22.2	274.9–381.5
	RDW-CV	RDW-SD	PLT	MPV	PDW	PCT	
Control	12.0±0.6	28.8±2.3	908.5±282.1	6.3±0.2	14.8±0.1	0.5±0.1	
CMSN	12.4±0.8	29.3±1.7	855.3±238.8	6.4±0.3	14.9±0.3	0.5±0.1	
Reference	6.8–13.3	12.5–47.3	276.1–1106.7	5.5–8.2	8.8–15.1	0.35–0.75	

Notes: Data were expressed as the mean ± SD.

Table 3 Effect of CMSN on Biochemical Parameters of Rats

	ALT	AST	ALP	DBIL	TBIL	ALB	TP
Control	31.5±7.5	97.4±35.9	143.6±29.2	1.1±0.4	1.4±0.6	38.7±3.9	56.4±2.9
CMSN	34.3±11.6	100.3±22.8	115.8±34.8	0.7±0.2	1.4±0.4	39.7±3.0	60.2±2.9*
Reference	33.7–98.7	69.7–322.9	1.3–221.0	0.2–1.2	0.4–1.6	31.7–43.7	54.2–85.7
	GLB	A/G	IBIL	BUN	CRE	UA	
Control	17.6±2.2	2.2±0.4	0.4±0.3	8.2±1.5	21.5±3.3	63.0±8.7	
CMSN	20.4±1.6*	1.9±0.2	0.5±0.2	7.6±1.1	22.0±4.1	70.8±11.5	
Reference	11.8–35.2	1.75–2.85	0–0.8	3.0–8.7	17.4–67.9	58.8–100.2	

Notes: Data were expressed as the mean ± SD. *P < 0.05 compared to the control group.

Funding

This work was supported by the National Natural Science Foundation of China (No. 81903550; No. 81773672), National Science and Technology Major Project [No. 2017ZX09101001-006-012], and the China Postdoctoral Science Foundation (No. 2018M641755).

Disclosure

The authors declare no conflicts of interest.

References

- Zhou Y, Quan G, Wu Q, et al. Mesoporous silica nanoparticles for drug and gene delivery. *Acta Pharm Sin B*. 2018;8(2):165–177. doi:10.1016/j.apsb.2018.01.007
- Croissant JG, Fatieiev Y, Almalik A, Khashab NM. Mesoporous silica and organosilica nanoparticles: physical chemistry, biosafety, delivery strategies, and biomedical applications. *Adv Healthc Mater*. 2018;7(4):1700831.
- Zhou HP, Gao SM, Zhang WW, An ZH, Chen DH. Dynamic adsorption of toluene on amino-functionalized SBA-15 type spherical mesoporous silica. *RSC Adv*. 2019;9(13):7196–7202. doi:10.1039/C8RA08605B
- Phillips KR, England GT, Sunny S, Shirman E, Shirman T, Vogel N. A colloidoscope of colloid-based porous materials and their uses. *Chem Soc Rev*. 2018;45(2):281–322.
- Perez RA, Singh RK, Kim TH, Kim HW. Silica-based multifunctional nanodelivery systems toward regenerative medicine. *Mater Horiz*. 2017;4:772–799. doi:10.1039/C7MH00017K
- Moodley T, Singh M. Polymeric mesoporous silica nanoparticles for enhanced delivery of 5-fluorouracil in vitro. *Pharmaceutics*. 2019;11(6):288–308. doi:10.3390/pharmaceutics11060288
- Wei Y, Gao L, Wang L, et al. Polydopamine and peptide decorated doxorubicin-loaded mesoporous silica nanoparticles as a targeted drug delivery system for bladder cancer therapy. *Drug Deliv*. 2017;24(1):681–691. doi:10.1080/10717544.2017.1309475
- Zhang W, Zheng N, Chen L, et al. Effect of shape on mesoporous silica nanoparticles for oral delivery of indomethacin. *Pharmaceutics*. 2019;11:4–16. doi:10.3390/pharmaceutics11010004
- Wang Y, Zhao Q, Han N, et al. Mesoporous silica nanoparticles in drug delivery and biomedical applications. *Nanomed Nanotechnol*. 2015;11(2):313–327. doi:10.1016/j.nano.2014.09.014
- Zheng N, Li J, Xu C, Xu L, Li S, Xu L. Mesoporous silica nanorods for improved oral drug absorption. *Artif Cell Nanomed B*. 2018;46(6):1132–1140. doi:10.1080/21691401.2017.1362414
- Li J, Xu L, Wang HY, et al. Comparison of bare and amino modified mesoporous silica@poly(ethyleneimine)s xerogel as indomethacin carrier: superiority of amino modification. *Mat Sci Eng C*. 2016;59:710–716. doi:10.1016/j.msec.2015.10.072
- Sun XX, Wang N, Yang LY, Ouyang XK, Huang FF. Folic acid and PEI modified mesoporous silica for targeted delivery of curcumin. *Pharmaceutics*. 2019;11(9):430. doi:10.3390/pharmaceutics11090430
- Sohmiya M, Saito K, Ogawa M. Host–guest chemistry of mesoporous silicas: precise design of location, density and orientation of molecular guests in mesopores. *Sci Technol Adv Mat*. 2015;16(5):054201. doi:10.1088/1468-6996/16/5/054201
- Adrian S, Magdalena P. Amino-modified mesoporous silica SBA-15 as bifunctional drug delivery system for cefazolin: release profile and mineralization potential. *Mater Lett*. 2018;227:136–140. doi:10.1016/j.matlet.2018.05.059
- Qiu L, Zhang W, Wang S, et al. Construction of multifunctional porous silica nanocarriers for ph/enzyme-responsive drug release. *Mat Sci Eng C*. 2017;81:485–491. doi:10.1016/j.msec.2017.08.029
- Li H, Wu X, Yang B, et al. Evaluation of biomimetically synthesized mesoporous silica nanoparticles as drug carriers: structure, wettability, degradation, biocompatibility and brain distribution. *Mat Sci Eng C*. 2019;94:453–464. doi:10.1016/j.msec.2018.09.053
- Lu F, Wu SH, Hung Y, Mou CY. Size effect on cell uptake in well-suspended, uniform mesoporous silica nanoparticles. *Small*. 2009;5(12):1408–1413. doi:10.1002/sml.200900005
- Li L, Liu T, Fu C, Tan L, Meng X, Liu H. Biodistribution, excretion, and toxicity of mesoporous silica nanoparticles after oral administration depend on their shape. *Nanomed Nanotechnol*. 2015;11(8):1915–1924. doi:10.1016/j.nano.2015.07.004
- Kim I, Joachim E, Choi H, Kim K. Toxicity of silica nanoparticles depends on size, dose, and cell type. *Nanomed Nanotechnol*. 2015;11(6):1407–1416. doi:10.1016/j.nano.2015.03.004
- Wang Y, Li W, Liu T, et al. Design and preparation of mesoporous silica carriers with chiral structures for drug release differentiation. *Mat Sci Eng C*. 2019;103:109737. doi:10.1016/j.msec.2019.109737
- Li H, Li H, Wei C, Ke J, Li J, Xu L. Biomimetic synthesis and evaluation of histidine-derivative templated chiral mesoporous silica for improved oral delivery of the poorly water-soluble drug, nimodipine. *Eur J Pharm Sci*. 2018;117:321–330. doi:10.1016/j.ejps.2018.03.013
- Li J, Xu L, Yang B, et al. Facile synthesis of functionalized ionic surfactant templated mesoporous silica for incorporation of poorly water-soluble drug. *Int J Pharm*. 2015;492(1–2):191–198. doi:10.1016/j.ijpharm.2015.07.014
- Li J, Du X, Zheng N, Xu L, Xu J, Li S. Contribution of carboxyl modified chiral mesoporous silica nanoparticles in delivering doxorubicin hydrochloride in vitro: ph-response controlled release, enhanced drug cellular uptake and cytotoxicity. *Colloid Surface B*. 2016;141:374–381. doi:10.1016/j.colsurfb.2016.02.009
- Ran F, Lei W, Cui Y, et al. Size effect on oral absorption in polymer-functionalized mesoporous carbon nanoparticles. *J Colloid Interf Sci*. 2017;511:57–66. doi:10.1016/j.jcis.2017.09.088
- Manne B, Thiruvayapati H, Bontha S, Motagondanahalli Rangarasaiah R, Das M, Balla VK. Surface design of mg-zn alloy temporary orthopaedic implants: tailoring wettability and biodegradability using laser surface melting. *Surf Coat Tech*. 2018;347:337–349. doi:10.1016/j.surfcoat.2018.05.017
- Carman ML, Estes TG, Feinberg AW, Schumacher JF, Wilkerson W, Wilson LH. Engineered antifouling microtopographies-correlating wettability with cell attachment. *Biofouling*. 2006;22(1):11–21. doi:10.1080/08927010500484854
- Tao S, Wang Y. Synthesis of hierarchically porous silica film with controllable surface wettability. *Int Nano Lett*. 2014;4(1):1–5. doi:10.1007/s40089-014-0102-y
- Zhu R, Wang Y, Zhang Z, Ma D, Wang X. Synthesis of polycarbonate urethane elastomers and effects of the chemical structures on their thermal, mechanical and biocompatibility properties. *Heliyon*. 2016;2(6):e00125. doi:10.1016/j.heliyon.2016.e00125
- He Q, Shi J, Zhu M, Chen Y, Chen F. The three-stage in vitro, degradation behavior of mesoporous silica in simulated body fluid. *Micropor Mesopor Mat*. 2010;131(1–3):314–320. doi:10.1016/j.micromeso.2010.01.009
- Parale VG, Mahadik DB, Mahadik SA, Kavale MS, Venkateswara Rao A, Wagh PB. Wettability study of surface modified silica aerogels with different silylating agents. *J Sol-Gel Sci Techn*. 2012;63(3):573–579. doi:10.1007/s10971-012-2788-5
- Singh A, Worku ZA, Guy VDM. Oral formulation strategies to improve solubility of poorly water-soluble drugs. *Expert Opin Drug Del*. 2011;8(10):1361–1378. doi:10.1517/17425247.2011.606808

32. Wang Y, Zhao Y, Cui Y, et al. Overcoming multiple gastrointestinal barriers by bilayer modified hollow mesoporous silica nanocarriers. *Acta Biomater.* 2018;65:405–416. doi:10.1016/j.actbio.2017.10.025
33. Fu C, Liu T, Li L, Liu H, Chen D, Tang F. The absorption, distribution, excretion and toxicity of mesoporous silica nanoparticles in mice following different exposure routes. *Biomaterials.* 2013;34(10):2565–2575. doi:10.1016/j.biomaterials.2012.12.043
34. Greish K, Thiagarajan G, Herd H, et al. Size and surface charge significantly influence the toxicity of silica and dendritic nanoparticles. *Nanotoxicology.* 2012;6(7):713–723. doi:10.3109/17435390.2011.604442
35. Yu T, Greish K, McGill LD, Ray A, Ghandehari H. Influence of geometry, porosity, and surface characteristics of silica nanoparticles on acute toxicity: their vasculature effect and tolerance threshold. *ACS Nano.* 2012;6(3):2289–2301. doi:10.1021/nn2043803
36. Lankoff A, Arabski M, Wegierek-Ciuk A, et al. Effect of surface modification of silica nanoparticles on toxicity and cellular uptake by human peripheral blood lymphocytes in vitro. *Nanotoxicology.* 2013;7(3):235–250. doi:10.3109/17435390.2011.649796
37. Yang Y, Zhou J, Detsch R, et al. Biodegradable nanostructures: degradation process and biocompatibility of iron oxide nanostructured arrays. *Mat Sci Eng C.* 2018;85:203–213. doi:10.1016/j.msec.2017.12.021
38. Gang X, Qian W, Zhang T, Yang X, Xia Q, Cheng D. Aurora b kinase is required for cell cycle progression in silkworm. *Gene.* 2017;599:60–67. doi:10.1016/j.gene.2016.11.015
39. Menti C, Beltrami M, Possan AL, Martins ST, Roesch-Ely M. Biocompatibility and degradation of gold-covered magneto-elastic biosensors exposed to cell culture. *Colloid Surface B.* 2016;143:111–117. doi:10.1016/j.colsurfb.2016.03.034
40. Zhen Z, Liu X, Huang T, Xi TF, Zheng Y. Hemolysis and cytotoxicity mechanisms of biodegradable magnesium and its alloys. *Mat Sci Eng C.* 2015;46:202–206. doi:10.1016/j.msec.2014.08.038
41. Dam DHM, Culver KSB, Kandela I, et al. Biodistribution and in vivo toxicity of aptamer-loaded gold nanostars. *Nanomed Nanotechnol.* 2015;11(3):671–679. doi:10.1016/j.nano.2014.10.005
42. Yu Q, Xiong XQ, Zhao L, et al. Biodistribution and toxicity assessment of superparamagnetic iron oxide nanoparticles in vitro and in vivo. *Curr Med Sci.* 2018;38(6):1096–1102. doi:10.1007/s11596-018-1989-8
43. Caster JM, Yu SK, Patel AN, et al. Effect of particle size on the biodistribution, toxicity, and efficacy of drug-loaded polymeric nanoparticles in chemoradiotherapy. *Nanomed Nanotechnol.* 2017;13(5):1673–1683. doi:10.1016/j.nano.2017.03.002
44. Samat S, Nor NA, Nor F, Ismail WI. Effects of gelam and acacia honey acute administration on some biochemical parameters of sprague dawley rats. *BMC Complement Altern Me.* 2014;14(1):146. doi:10.1186/1472-6882-14-146

International Journal of Nanomedicine

Dovepress

Publish your work in this journal

The International Journal of Nanomedicine is an international, peer-reviewed journal focusing on the application of nanotechnology in diagnostics, therapeutics, and drug delivery systems throughout the biomedical field. This journal is indexed on PubMed Central, MedLine, CAS, SciSearch®, Current Contents®/Clinical Medicine,

Journal Citation Reports/Science Edition, EMBase, Scopus and the Elsevier Bibliographic databases. The manuscript management system is completely online and includes a very quick and fair peer-review system, which is all easy to use. Visit <http://www.dovepress.com/testimonials.php> to read real quotes from published authors.

Submit your manuscript here: <https://www.dovepress.com/international-journal-of-nanomedicine-journal>